LETTER

doi:10.1038/nature11729

NLRP3 is activated in Alzheimer's disease and contributes to pathology in APP/PS1 mice

Michael T. Heneka[1,2]*, Markus P. Kummer[1], Andrea Stutz[3], Andrea Delekate[4], Stephanie Schwartz[1], Ana Vieira-Saecker[1], Angelika Griep[1], Daisy Axt[1], Anita Remus[4], Te-Chen Tzeng[5], Ellen Gelpi[6], Annett Halle[7], Martin Korte[4,8], Eicke Latz[2,3,5]* & Douglas T. Golenbock[5]*

Alzheimer's disease is the world's most common dementing illness. Deposition of amyloid-β peptide drives cerebral neuroinflammation by activating microglia[1,2]. Indeed, amyloid-β activation of the NLRP3 inflammasome in microglia is fundamental for interleukin-1β maturation and subsequent inflammatory events[3]. However, it remains unknown whether NLRP3 activation contributes to Alzheimer's disease *in vivo*. Here we demonstrate strongly enhanced active caspase-1 expression in human mild cognitive impairment and brains with Alzheimer's disease, suggesting a role for the inflammasome in this neurodegenerative disease. *Nlrp3*$^{-/-}$ or *Casp1*$^{-/-}$ mice carrying mutations associated with familial Alzheimer's disease were largely protected from loss of spatial memory and other sequelae associated with Alzheimer's disease, and demonstrated reduced brain caspase-1 and interleukin-1β activation as well as enhanced amyloid-β clearance. Furthermore, NLRP3 inflammasome deficiency skewed microglial cells to an M2 phenotype and resulted in the decreased deposition of amyloid-β in the APP/PS1 model of Alzheimer's disease. These results show an important role for the NLRP3/caspase-1 axis in the pathogenesis of Alzheimer's disease, and suggest that NLRP3 inflammasome inhibition represents a new therapeutic intervention for the disease.

The chronic deposition of amyloid-β stimulates the persistent activation of microglial cells in Alzheimer's disease[1]. Increased interleukin (IL)-1β amounts have been implicated in the response to amyloid-β deposition[2]. IL-1β is produced as a biologically inactive pro-form and requires caspase-1 for activation and secretion. Caspase-1 activity is controlled by inflammasomes, sensors of microbial components and sterile danger signals. The NLRP3 inflammasome has been implicated in several chronic inflammatory diseases as it can sense inflammatory crystals and aggregated proteins, including amyloid-β[3,4]. Because of the possibility that the neuroinflammatory component of Alzheimer's disease involves inflammasome activation, we assessed the cleavage of caspase-1 in brains from patients with Alzheimer's disease, early-onset Alzheimer's disease and mild cognitive impairment. We observed substantially increased amounts of cleaved caspase-1 in hippocampal or cortical lysates from those patients' brains compared with controls (Fig. 1a and Supplementary Fig. 1), consistent with chronic inflammasome activation[4]. This increase of caspase-1 processing was mirrored in aged APP/PS1 transgenic mice (Fig. 1b). APP/PS1 mice express a human/mouse chimaeric amyloid precursor protein and human presenilin-1, each carrying mutations associated with familial Alzheimer's disease[5], leading to the chronic deposition of amyloid-β, neuroinflammation and cognitive impairment.

Nlrp3$^{-/-}$ mice were crossed into APP/PS1 mice to obtain APP/PS1/*Nlrp3*$^{-/-}$ mice to assess the contribution of the NLRP3 inflammasome to the pathogenesis of Alzheimer's disease. In APP/PS1/*Nlrp3*$^{-/-}$ mice, caspase-1 cleavage was absent. Total brain IL-1β amounts were similar to those in wild-type (WT) animals (Fig. 1b, c). Immunohistochemistry for the inflammasome component ASC detected microglial 'speck' formation in activated (Iba1^{+}) microglia cells from APP/PS1 mice, consistent with inflammasome activation (Fig. 1d). We assessed spatial memory formation in age-matched 16-month-old WT, *Nlrp3*$^{-/-}$, *Casp1*$^{-/-}$, APP/PS1, APP/PS1/*Nlrp3*$^{-/-}$ and APP/PS1/*Casp1*$^{-/-}$ mice using the Morris water-maze test including probe trial testing. As expected, aged APP/PS1 mice showed severe deficits in spatial memory formation. However, APP/PS1/*Nlrp3*$^{-/-}$ and APP/PS1/*Casp1*$^{-/-}$ mice were largely protected from spatial memory impairment (Fig. 1e, f and Supplementary Figs 2–9). These results were supported by object recognition memory testing (Supplementary Fig. 10). Again, NLRP3- or caspase-1-deficient APP/PS1 mice were protected from memory deficits (Supplementary Fig. 10). To assess the effect of NLRP3 or caspase-1 gene deficiency on neuronal function in murine Alzheimer's disease, we determined hippocampal synaptic plasticity, which is considered to represent the basis of newly formed declarative memories and is often analysed by measuring long-term potentiation (LTP)[6,7]. NLRP3 or caspase-1 deficiency completely prevented LTP suppression in hippocampal slices from APP/PS1 mice (Fig. 1g and Supplementary Fig. 11). Baseline synaptic transmission and short-term plasticity (measured as paired-pulse facilitation) were unaltered (Supplementary Fig. 12). An analysis of spine morphology showed a small but statistically significant reduction of spine density in the pyramidal neurons of APP/PS1 mice, which was prevented by NLRP3 or caspase-1 deficiency (Supplementary Fig. 13). The small degree of spine density reduction suggested that LTP suppression in APP/PS1 mice was primarily mediated by functional rather than structural changes. Body weight and blood glucose amounts were similar between groups of mice (Supplementary Fig. 14). Behavioural analysis in the open field arena verified increased locomotion and slowed habituation in APP/PS1 mice, similar to previous reports[8]. APP/PS1/*Nlrp3*$^{-/-}$ mice, however, had a reduced hyperdynamic phenotype and normalized habituation (Fig. 1h and Supplementary Fig. 15), suggesting that NLRP3 deficiency improved neurobehavioural disturbances such as Alzheimer's-disease-like psychomotor disinhibition. These results support a fundamental role for NLRP3/caspase-1-mediated inflammation in behavioural and cognitive dysfunction in Alzheimer's disease.

Alzheimer's-disease-associated inflammation interferes with APP metabolism and with mechanisms of amyloid-β aggregation and clearance at several levels[9,10]. Thioflavin S staining showed a marked decrease in hippocampal and cortical amyloid-β deposition in the APP/PS1/*Nlrp3*$^{-/-}$ mice (Fig. 2a, b and Supplementary Fig. 16). Additionally, APP/PS1/*Nlrp3*$^{-/-}$ mice showed a 70% reduction in brain concentrations of highly aggregated, formic-acid-extractable

[1]Clinical Neuroscience Unit, Department of Neurology, University of Bonn, Sigmund-Freud-Strasse 25, 53127 Bonn, Germany. [2]Deutsches Zentrum für Neurodegenerative Erkrankungen (DZNE), 53175 Bonn, Germany. [3]Institute of Innate Immunity, University of Bonn, 53127 Bonn, Germany. [4]Division of Cellular Neurobiology, Zoological Institute, Technische Universität Braunschweig, 38106 Braunschweig, Germany. [5]Department of Medicine and Division of Infectious Diseases and Immunology, University of Massachusetts Medical School, Worcester 01605, Massachusetts, USA. [6]Neurological Tissue Bank, University of Barcelona-Hospital Clinic, IDIBAPS, 08036 Barcelona, Spain. [7]Center for Advanced European Studies and Research-CAESAR, 53175 Bonn, Germany. [8]Helmholtz-Center for Infection Research, HZI, AG NIND, 38124 Braunschweig, Germany.
*These authors contributed equally to this work.

©2013 Macmillan Publishers Limited. All rights reserved

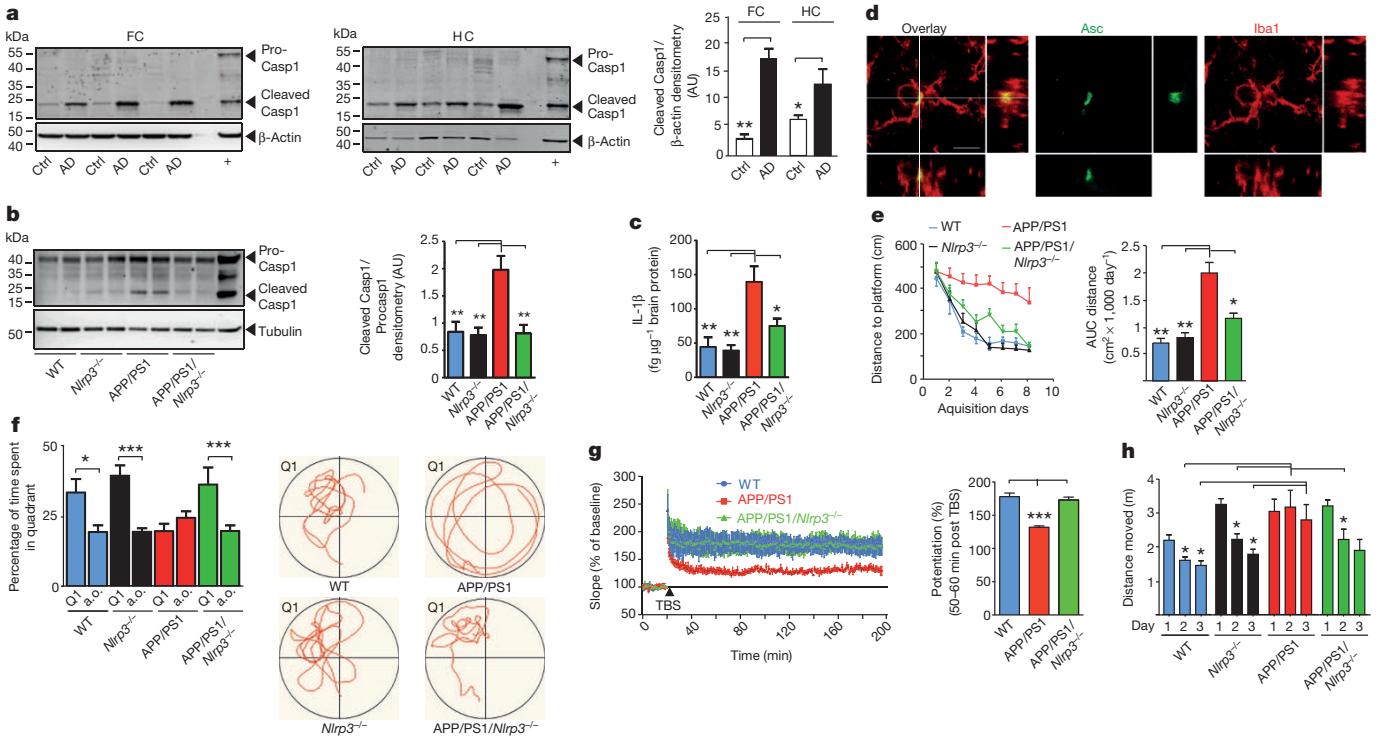

Figure 1 | Protective effects of NLRP3 gene deficiency in APP/PS1 mice on memory and behaviour. **a**, Western blot and quantification of cleaved caspase-1 in brain lysates from frontal cortex (FC) and hippocampus (HC) of patients with Alzheimer's disease (AD, $n = 12$) and controls (Ctrl, $n = 8$) (mean ± s.e.m., Student's *t*-test, $*P < 0.05$, $**P < 0.01$; + is positive control). **b**, Western blot of cleaved caspase-1 and quantification in mice at 16 months ($n = 5$, mean ± s.e.m., analysis of variance (ANOVA), Tukey's (*post hoc*) test, $**P < 0.01$). AU, arbitrary units. **c**, Parenchymal IL-1β in mouse brains from **b** ($n = 5$, mean ± s.e.m., ANOVA, Tukey's test, $*P < 0.05$, $**P < 0.01$). **d**, Immunohistochemistry of microglia from APP/PS1 mice for Iba1 (red) and Asc (green). Scale bar, 10 μm. **e**, Morris water-maze analysis as distance travelled (centimetres) and integrated distance (AUC) for WT ($n = 16$), *Nlrp3*$^{-/-}$ ($n = 12$), APP/PS1 ($n = 14$) and APP/PS1/*Nlrp3*$^{-/-}$ ($n = 15$) mice (mean ± s.e.m., ANOVA, Tukey's test, $*P < 0.05$, $**P < 0.01$). **f**, Probe trial day 9. Q1, quadrant where platform was located on days 1–8. Time spent in all other (a.o.) quadrants was averaged for all of the above mice (mean ± s.e.m.; one-way ANOVA, Tukey's test, $*P < 0.05$, $***P < 0.001$). Representative runs (right panels). **g**, LTP was induced by theta-burst stimulation (TBS) 20 min after baseline recordings in hippocampal slices from mice. LTP is expressed as percentage potentiation of baseline (100%) and the significance is determined 55–60 min after the TBS was given (mean of WT $n = 16$, APP/PS1 $n = 23$, APP/PS1/*Nlrp3*$^{-/-}$ $n = 16$; hippocampal slices measured ± s.e.m. from $n = 6$–9 animals per group; ANOVA, Tukey's test, $***P < 0.001$). **h**, Open field test, age = 16 months. Vertical locomotor activity (distance travelled) decreased over three consecutive days in WT ($n = 16$) and *Nlrp3*$^{-/-}$ ($n = 12$) mice. Habituation was not observed in APP/PS1 mice showing a hyperdynamic behavioural phenotype. APP/PS1/*Nlrp3*$^{-/-}$ mice ($n = 15$) were indistinguishable from *Nlrp3*$^{-/-}$ mice ($n = 12$) (mean ± s.e.m., ANOVA, Tukey's test, $*P < 0.05$).

forms of amyloid-β (Fig. 2c). This reduction was most probably not due to changes of APP expression and processing, as formation of carboxy (C)-terminal fragments or amounts of β-secretase-1 (BACE1) messenger RNA (mRNA) and protein (Fig. 2 and Supplementary Fig. 17) were unaffected in NLRP3 knockout mice. This conclusion was further strengthened by the analysis of 4-month-old APP/PS1 mice; neither NLRP3 nor caspase-1 deficiency influenced amyloid-β amounts (Supplementary Fig. 18). However, aggregated forms of amyloid-β were markedly reduced in the APP/PS1/*Nlrp3*$^{-/-}$ mice, as shown by the further quantification of amyloid-β species by enzyme-linked immunosorbent assay (ELISA). These studies showed a strong reduction of amyloid-β_{1-40} and amyloid-β_{1-42} in the APP/PS1/*Nlrp3*$^{-/-}$ mice after sequential extraction by radio-immunoprecipitation assay (RIPA) and sodium dodecyl sulphate (SDS) buffer, allowing the analysis of soluble and insoluble amyloid-β (Fig. 2d). At 16 months of age, amyloid-β_{1-38} was only detectable in SDS extracts. Again, analysis of the APP/PS1/*Nlrp3*$^{-/-}$ mice showed reduced amounts compared with APP/PS1 mice (Supplementary Fig. 19). Analysis of cerebral amyloid-β amounts of APP/PS1 and APP/PS1/*Casp1*$^{-/-}$ mice showed that caspase-1 deficiency resulted in similar changes in amyloid-β, suggesting that NLRP3 acts through caspase-1 to exert the observed effects (Supplementary Figs 20 and 21).

As both amyloid-β and IL-1β have been implicated in the suppression of LTP[11–13], their reduction may jointly contribute to the protection of LTP, improved spatial memory and normalized behaviour in the NLRP3-deficient APP/PS1 mice.

Microglia are found in increased numbers in close proximity to amyloid-β plaques in Alzheimer's disease. Microglia assembly in the vicinity of plaques is interpreted as an attempt to clear the pathological deposits of amyloid-β through phagocytosis and degradation. The functional impact of phagocytosis is highlighted by studies showing that restricting microglial accumulation and phagocytosis increases amyloid-β deposition[14,15]. As Alzheimer's disease progresses, microglial cells adopt a chronically activated phenotype. Cytokines, including IL-1β, were found to impair microglial clearance functions[16,17]. Likewise, suppression of inflammatory cytokine production resets microglial phagocytosis in APP/PS1 mice[17]. We analysed the impact of NLRP3 or caspase-1 deficiency on the phagocytic capacity of microglia *in vivo* because immunohistochemistry showed microglial ASC and NLRP3 expression (Fig. 1d and Supplementary Figs 22 and 23a). In addition, we observed that inflammasome activation occurred in an age- and amyloid-β deposition-related fashion (Supplementary Figs 23b and 24). We administered a fluorescent derivative of Congo red known as methoxy-XO4, which crosses the blood–brain barrier and has nanomolar binding affinity for amyloid-β. We injected methoxy-XO4 into adult APP/PS1, APP/PS1/*Nlrp3*$^{-/-}$ and APP/PS1/*Casp1*$^{-/-}$ mice. Three hours after injection, methoxy-XO4 fluorescence in brain homogenates did not differ between groups (Supplementary Fig. 25). At this

©2013 Macmillan Publishers Limited. All rights reserved

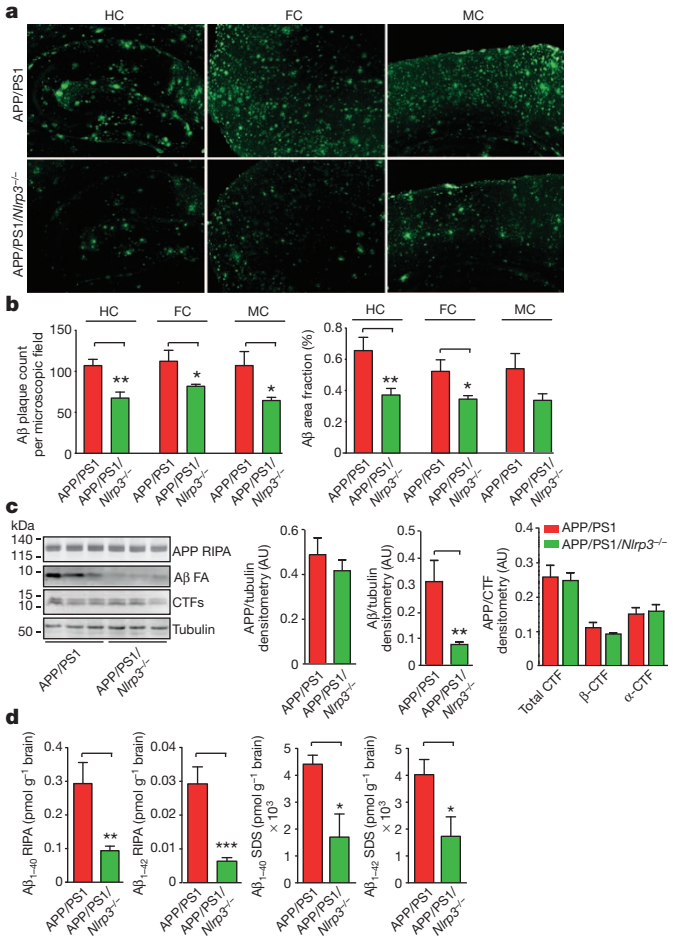

Figure 2 | NLRP3 gene deficiency leads to decreased amyloid-β amounts and deposition. **a**, Amyloid-β plaque deposition was quantified in the hippocampus (HC), frontal cortex (FC) and motor cortex (MC) using thioflavin S. **b**, Quantification of number and surface area of amyloid-β (Aβ) plaques was performed in five consecutive sections per animal and is given as count per area or area fraction (%) ($n = 7$–8, mean ± s.e.m., Students t-test, $^*P < 0.05$, $^{**}P < 0.001$). **c**, Western blot analysis of RIPA and formic-acid (FA) brain extracts of 16-month-old APP/PS1 ($n = 3$) and APP/PS1/$Nlrp3^{-/-}$ ($n = 3$) mice. Densitometrical quantification of APP, formic-acid-soluble amyloid-β and carboxyl-terminal fragments (CTFs) as ratios ($n = 5$, mean ± s.e.m., Student's t-test, $^{**}P < 0.01$). **d**, ELISA of RIPA and SDS fractions for amyloid-β_{1-40} and amyloid-β_{1-42} from 16-month-old mice ($n = 5$, mean ± s.e.m., Student's t-test, $^*P < 0.05$, $^{**}P < 0.01$, $^{***}P < 0.001$).

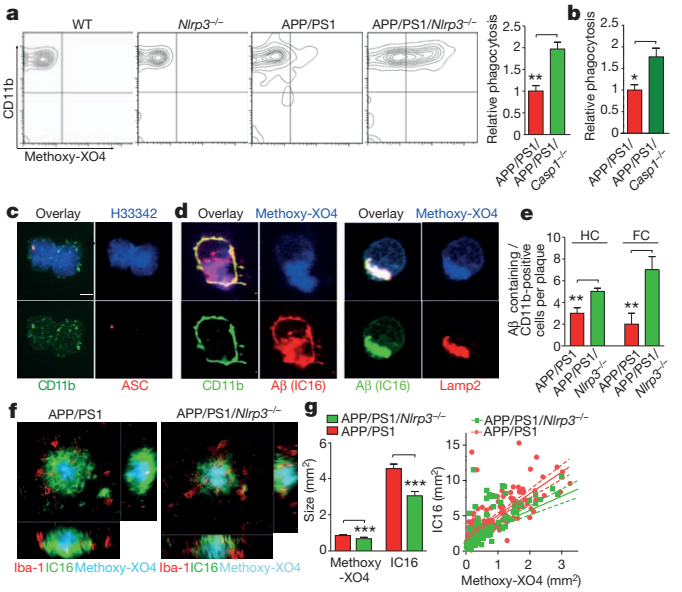

Figure 3 | NLRP3 or caspase-1 deficiency increases microglial amyloid-β phagocytosis. **a**, Quantification of amyloid-β phagocytosis by flow cytometry of microglia isolated from adult mice 3 h after intraperitoneal injection of methoxy-XO4 ($n = 5$, mean ± s.e.m., ANOVA, Tukey's test, $^{**}P < 0.01$). **b**, Same as **a** with APP/PS1 and APP/PS1/$Casp1^{-/-}$ mice ($n = 5$, mean ± s.e.m., ANOVA, Tukey's test, $^*P < 0.05$). **c**, Immunohistochemistry staining of ASC specks in $CD11b^+$ microglia. H33342 is a nuclear stain. **d**, Immunocytochemistry of monoclonal antibody IC16 (anti-amyloid-β), methoxy-XO4 labelled amyloid-β within $Lamp2^+$ intracellular structures in $CD11b^+$ microglia from 16-month-old APP/PS1 mice. **e**, Quantification of $CD11b^+$, amyloid-β^+ microglia in the hippocampus (HC) and frontal cortex (FC) of 16-month-old mice ($n = 5$, mean ± s.e.m., Student's t-test, $^{**}P < 0.01$). **f**, Representative micrographs from methoxy-XO4-treated APP/PS1 and APP/PS1/$Nlrp3^{-/-}$ mice stained for Iba-1 and amyloid-β. **g**, Average IC16-positive amyloid-β plaque size, determined by co-labelling with methoxy-XO4, was markedly reduced in APP/PS1/$Nlrp3^{-/-}$ mice (150 plaques were assessed from each group of four mice, mean ± s.e.m., Student's t-test, $^{***}P < 0.001$). A scatter plot of all plaques that was analysed by linear regression is shown at the right (150 plaques per group; lines: linear regression analysis; dashed lines: 95% confidence intervals, $R^2 = 0.5588$ for APP/PS1 and $R^2 = 0.4431$ for APP/PS1/$Nlrp3^{-/-}$ mice).

point, mice were euthanized and microglial cells were isolated and analysed for methoxy-XO4 fluorescence by flow cytometry. An increase of nearly twofold in amyloid-β phagocytosis was found in APP/PS1/$Nlrp3^{-/-}$ or APP/PS1/$Casp1^{-/-}$ compared with APP/PS1 mice (Fig. 3a, b), suggesting that NLRP3/caspase-1 inflammasome activation reduces amyloid-β phagocytosis. Microglia were isolated from brains by cytospin. Co-immunostaining again showed microglial ASC speck formation (Fig. 3c). Methoxy-XO4 labelled amyloid-β was detected within $CD11b^+$ microglia and co-localized to Lamp2-positive, amyloid-β-containing lysosomes (Fig. 3d and Supplementary Fig. 26). Notably, increased uptake of methoxy-XO4 labelled amyloid-β was associated with enhanced CD36 expression (Supplementary Fig. 27). Although the methoxy-XO4 assay cannot functionally distinguish between increased phagocytosis and impaired degradation, we performed further microscopy. This showed that NLRP3 deficiency substantially altered the characteristics of amyloid-β plaque deposition (Fig. 3e, f and Supplementary Fig. 28). First, the total volume of the amyloid-β plaque was reduced in APP/PS1/$Nlrp3^{-/-}$ mice compared with APP/PS1 mice (Fig. 3g). Second, APP/PS1/$Nlrp3^{-/-}$ mice showed more reduction in the outer parts of the amyloid-β plaque than in the core. Furthermore, microglial cells surrounding amyloid-β plaques in APP/PS1 mice phagocytosed amyloid-β to a lesser extent (Fig. 3e, g and Supplementary Fig. 29). Together with the documented suppression of microglial phagocytosis by proinflammatory cytokines, these data argue for an increase in phagocytosis in APP/PS1/$Nlrp3^{-/-}$ mice. These results may be surprising, because they seemingly contradict a report that experimental local overproduction of IL-1β reduced amyloid-β deposition[18]. However, there are two explanations for these apparently opposite results. First, the NLRP3/caspase-1-axis may use substrates other than IL-1β to constrain microglial amyloid-β phagocytosis. Second, it is likely that the experimental approach that was used by Shaftel *et al.* disrupted the blood–brain barrier, allowing amyloid-β removal by peripherally derived myeloid cells[19]. Similar effects on amyloid-β plaque metabolism have been observed after whole-body irradiation, which also leads to disruption of the blood–brain barrier[1]. Shielding the APP/PS1 brain from radiation restricted the infiltration of peripheral cells to a level that did not significantly contribute to the clearance of parenchymal amyloid-β[20].

In addition to phagocytosis, microglia also contribute to amyloid-β clearance through proteolytic enzymes, including insulin-degrading enzyme (IDE) and neprilysin (NEP)[21]. Cerebral homogenates from APP/PS1/$Nlrp3^{-/-}$ or APP/PS1/$Casp1^{-/-}$ mice demonstrated an increase of IDE whereas NEP amounts remained unchanged (Fig. 4a and Supplementary Fig. 30). Microglial cells purified from

©2013 Macmillan Publishers Limited. All rights reserved

16-month-old mice were one source of increased IDE transcription (Fig. 4b). Previous work established that a twofold increase of IDE expression is sufficient to reduce amyloid-β deposition strongly[22]. It is likely that the IDE increase enhances the degradation of amyloid-β and the overall amyloid-β reduction in inflammasome-deficient mice. These data suggest that NLRP3 activation negatively affects the microglial clearance function in Alzheimer's disease. Notably, recent evidence suggests that impaired clearance may be the driving force behind sporadic Alzheimer's disease[23], which constitutes the overwhelming majority of cases of human Alzheimer's disease.

Prolonged exposure to amyloid-β leads to persistent activation of microglial cells in Alzheimer's disease. On the basis of gene expression profiles, activated microglial cells may be divided into several different populations. The M1 and M2 subtypes represent the extremes of the range. Markers of alternatively activated microglia of the M2 subtype[24], including 'found in inflammatory zone 1' (FIZZ1) (Supplementary Fig. 31), arginase-1 and interleukin-4, showed increased expression in APP/PS1/*Nlrp3*$^{-/-}$ and APP/PS1/*Casp1*$^{-/-}$ mice (Fig. 4c–e). In contrast, cerebral nitric oxide synthase 2 (NOS2), a hallmark of the classically activated M1 proinflammatory phenotype, was reduced in inflammasome-deficient APP/PS1 mice (Fig. 4f, g). Thus, NLRP3- or caspase-1-deficiency results in a skewing of activated microglial cells towards an M2-like activated state. This M2 phenotype is also characterized by increased amyloid-β clearance and enhanced tissue remodelling. In Alzheimer's disease, the upregulation of NOS2 results in tyrosine nitration of several proteins, including amyloid-β, thereby accelerating its aggregation and seeding of new plaques[25]. In agreement with this, APP/PS1/*Nlrp3*$^{-/-}$ mice had less nitrated amyloid-β and a reduced average plaque size as well as fewer nitrated plaque cores (Fig. 4h–j). Because NO and nitrated amyloid-β act as strong LTP suppressors[25,26], a reduction of NOS2 and nitrated amyloid-β (Fig. 4g, j) should contribute to the protection of synaptic plasticity, memory and behaviour.

These data are consistent with the hypothesis that amyloid-β-induced activation of the NLRP3 inflammasome enhances Alzheimer's disease progression by mediating a harmful chronic inflammatory tissue response. Inflammatory mediators that result from NLRP3 inflammasome activation are probably involved in mediating synaptic dysfunction, cognitive impairment and the restriction of beneficial microglial clearance functions. This key role of the NLRP3 inflammasome in amyloid-β-mediated inflammatory responses suggests that a therapeutic that blocks the activity of the NLRP3 inflammasome, or inflammasome-derived cytokines, might effectively interfere with the progression of Alzheimer's disease.

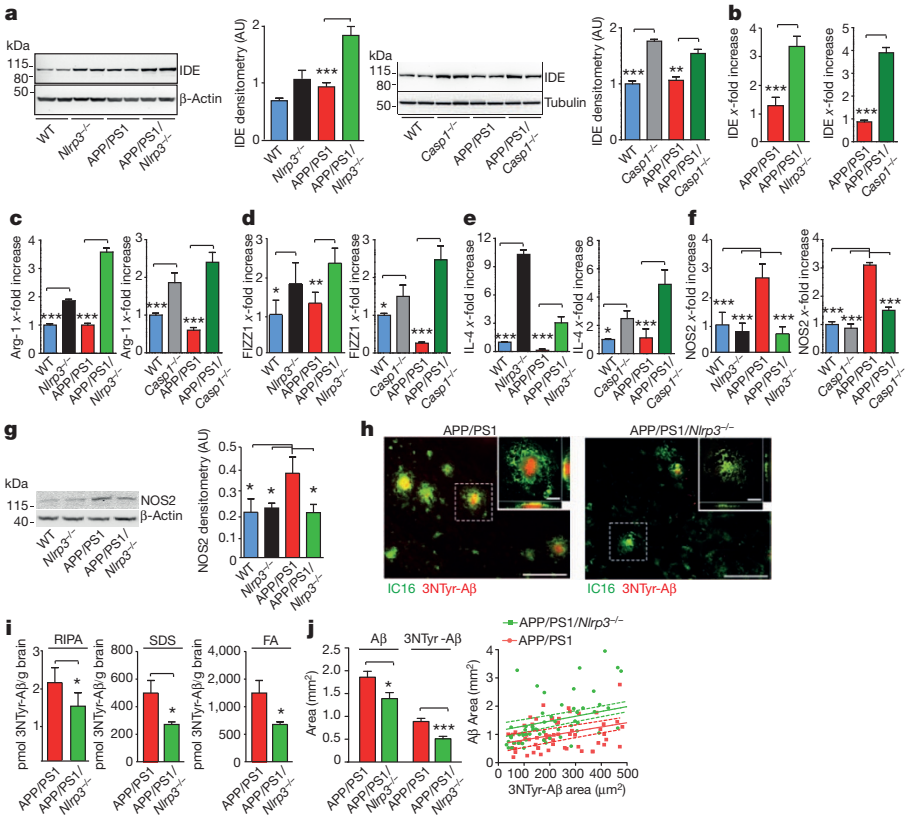

Figure 4 | NLRP3 gene deficiency conveys a M2 microglial phenotype, decreases NOS2 expression and strongly reduces 3NTyr-amyloid-β formation. **a**, Western blot detection of IDE in cerebral lysates of mice at 16 months of age. Quantification by densitometry is to the right of each western blot ($n = 5$, mean ± s.e.m., ANOVA, Tukey's test, $^{**}P < 0.01$, $^{***}P < 0.01$). **b**, Corresponding analysis of IDE gene transcription in caspase-1-deficient mice ($n = 5$ per group, mean ± s.e.m., Student's *t*-test, $^{***}P < 0.001$). **c**, Transcription of arginase-1 (Arg-1), (**d**) found in inflammatory zone-1 (FIZZ1), (**e**) IL-4 and (**f**) NOS2 at 16 months of age ($n = 5$, mean ± s.e.m., ANOVA, Tukey's *post hoc* test, $^{*}P < 0.05$, $^{**}P < 0.01$, $^{***}P < 0.01$). **g**, Western blot detection and quantification of NOS2 in cerebral lysates from 16-month-old mice ($n = 5$, mean ± s.e.m., ANOVA, Tukey's *post hoc* test, $^{*}P < 0.05$). **h**, Representative brain sections were analysed by immunohistochemistry for nitrated amyloid-β (3NTyr-Aβ). **i**, ELISA detection of 3-NTyr-Aβ in RIPA, SDS and formic-acid extracts showed a robust reduction of 3NTyr-Aβ in APP/PS1/*Nlrp3*$^{-/-}$ mice at 16 months ($n = 4$–5, Student's *t*-test, $^{*}P < 0.05$). **j**, Left: cortical sections from 16-month-old mice were probed for 3NTyr-Aβ and amyloid-β using monoclonal antibody IC16. NLRP3 gene deficiency reduced both IC16-positive amyloid-β and 3NTyr-Aβ plaque size (85 plaques were assessed from each group of four mice, mean ± s.e.m., Student's *t*-test, $^{*}P < 0.05$, $^{***}P < 0.001$). Right: scatter plot of all plaques analysed by linear regression ($n = 4$ mice, 85 plaques per group; lines: linear regression analysis; dashed lines: 95% confidence intervals, $R^2 = 0.4920$ for APP/PS1 and $R^2 = 0.3884$ APP/PS1/*Nlrp3*$^{-/-}$ mice).

©2013 Macmillan Publishers Limited. All rights reserved

METHODS SUMMARY

Caspase-1 activation of human and mouse brain tissue was analysed by western blot of cleaved caspase-1. IL-1β was quantified by ELISA. Microglial ASC speck formation was detected by immunohistochemistry. All mice were on C57/Bl6 background, including WT, *Nlrp3*$^{-/-}$ (ref. 27), APP/PS1 (ref. 5), APP/PS1/*Nlrp3*$^{-/-}$, *Casp1*$^{-/-}$ (ref. 28) and APP/PS1/*Casp1*$^{-/-}$, and were analysed for cognitive function using the Morris water-maze test, the object recognition test and open field behavioural testing. Synaptic plasticity was determined by measuring LTP in acutely isolated hippocampal slices. Spine density was assessed by analysing mid-apical dendritic sections of pyramidal CA1 neurons. Cerebral amyloid-β load was determined by thioflavin S immunohistochemistry of serial sections. Sequential extraction of homogenized brains by radio-immunoprecipitation assay, sodium dodecyl sulphate buffer and formic acid was used to determine amounts of amyloid-β. Amyloid-β nitration was determined by ELISA and immunohistochemistry using specific antibodies against 3NTyr^{10}-amyloid-β^{25}. Western blot detection was used to analyse the protein amounts of APP, carboxyl-terminal fragments, amyloid-β, BACE1, IDE and NOS2. Inflammasome activation was confirmed by detection of ASC speck formation in microglia isolated from adult mouse. Microglial amyloid-β phagocytosis was determined after peripheral injection of methoxy-XO4, isolation of microglia and subsequent FACS analysis. Confirmatory immunocytochemistry was performed using antibody IC16 and the lysosomal marker LAMP2. Plaque morphology and microglial amyloid-β uptake were analysed by coimmunostaining with Iba-1, methoxy-XO4 and IC16. mRNA amounts of IDE, NEP, M1 and M2 markers were determined either from sorted microglia or from brain tissue by quantitative PCR.

Full Methods and any associated references are available in the online version of the paper.

Received 26 February; accepted 30 October 2012.

Published online 19 December 2012; corrected online 30 January 2013 (see full-text HTML version for details).

1. Prinz, M., Priller, J., Sisodia, S. S. & Ransohoff, R. M. Heterogeneity of CNS myeloid cells and their roles in neurodegeneration. *Nature Neurosci.* **14,** 1227–1235 (2011).
2. Lucin, K. M. & Wyss-Coray, T. Immune activation in brain aging and neurodegeneration: too much or too little? *Neuron* **64,** 110–122 (2009).
3. Halle, A. *et al.* The NALP3 inflammasome is involved in the innate immune response to amyloid-β. *Nature Immunol.* **9,** 857–865 (2008).
4. Martinon, F., Mayor, A. & Tschopp, J. The inflammasomes: guardians of the body. *Annu. Rev. Immunol.* **27,** 229–265 (2009).
5. Jankowsky, J. L. *et al.* Co-expression of multiple transgenes in mouse CNS: a comparison of strategies. *Biomol. Eng.* **17,** 157–165 (2001).
6. Bliss, T. V. & Collingridge, G. L. A synaptic model of memory: long-term potentiation in the hippocampus. *Nature* **361,** 31–39 (1993).
7. Ho, V. M., Lee, J.-A. & Martin, K. C. The cell biology of synaptic plasticity. *Science* **334,** 623–628 (2011).
8. Walker, J. M. *et al.* Spatial learning and memory impairment and increased locomotion in a transgenic amyloid precursor protein mouse model of Alzheimer's disease. *Behav. Brain Res.* **222,** 169–175 (2011).
9. Heneka, M. T. & O'Banion, M. K. Inflammatory processes in Alzheimer's disease. *J. Neuroimmunol.* **184,** 69–91 (2007).
10. Lee, C. Y. D. & Landreth, G. E. The role of microglia in amyloid clearance from the AD brain. *J. Neural Transm.* **117,** 949–960 (2010).
11. Nalbantoglu, J. *et al.* Impaired learning and LTP in mice expressing the carboxy terminus of the Alzheimer amyloid precursor protein. *Nature* **387,** 500–505 (1997).
12. Chapman, P. F. *et al.* Impaired synaptic plasticity and learning in aged amyloid precursor protein transgenic mice. *Nature Neurosci.* **2,** 271–276 (1999).
13. Murray, C. A. & Lynch, M. A. Evidence that increased hippocampal expression of the cytokine interleukin-1β is a common trigger for age- and stress-induced impairments in long-term potentiation. *J. Neurosci.* **18,** 2974–2981 (1998).
14. El Khoury, J. *et al.* Ccr2 deficiency impairs microglial accumulation and accelerates progression of Alzheimer-like disease. *Nature Med.* **13,** 432–438 (2007).
15. Bamberger, M. E., Harris, M. E., McDonald, D. R., Husemann, J. & Landreth, G. E. A cell surface receptor complex for fibrillar β-amyloid mediates microglial activation. *J. Neurosci.* **23,** 2665–2674 (2003).
16. Hickman, S. E., Allison, E. K. & Khoury, J. E. Microglial dysfunction and defective β-amyloid clearance pathways in aging Alzheimer's disease mice. *J. Neurosci.* **28,** 8354–8360 (2008).
17. Heneka, M. T. *et al.* Locus ceruleus controls Alzheimer's disease pathology by modulating microglial functions through norepinephrine. *Proc. Natl Acad. Sci. USA* **107,** 6058–6063 (2010).
18. Shaftel, S. S. *et al.* Sustained hippocampal IL-1β overexpression mediates chronic neuroinflammation and ameliorates Alzheimer plaque pathology. *J. Clin. Invest.* **117,** 1595–1604 (2007).
19. Shaftel, S. S. *et al.* Chronic interleukin-1β expression in mouse brain leads to leukocyte infiltration and neutrophil-independent blood brain barrier permeability without overt neurodegeneration. *J. Neurosci.* **27,** 9301–9309 (2007).
20. Mildner, A. *et al.* Distinct and non-redundant roles of microglia and myeloid subsets in mouse models of Alzheimer's disease. *J. Neurosci.* **31,** 11159–11171 (2011).
21. Malito, E., Hulse, R. E. & Tang, W.-J. Amyloid β-degrading cryptidases: insulin degrading enzyme, neprilysin, and presequence peptidase. *Cell. Mol. Life Sci.* **65,** 2574–2585 (2008).
22. Leissring, M. A. *et al.* Enhanced proteolysis of β-amyloid in APP transgenic mice prevents plaque formation, secondary pathology, and premature death. *Neuron* **40,** 1087–1093 (2003).
23. Mawuenyega, K. G. *et al.* Decreased clearance of CNS β-amyloid in Alzheimer's disease. *Science* **330,** 1774 (2010).
24. Raes, G. *et al.* FIZZ1 and Ym as tools to discriminate between differentially activated macrophages. *Dev. Immunol.* **9,** 151–159 (2002).
25. Kummer, M. P. *et al.* Nitration of tyrosine 10 critically enhances amyloid β aggregation and plaque formation. *Neuron* **71,** 833–844 (2011).
26. Wang, Q., Rowan, M. J. & Anwyl, R. β-Amyloid-mediated inhibition of NMDA receptor-dependent long-term potentiation induction involves activation of microglia and stimulation of inducible nitric oxide synthase and superoxide. *J. Neurosci.* **24,** 6049–6056 (2004).
27. Kanneganti, T.-D. *et al.* Bacterial RNA and small antiviral compounds activate caspase-1 through cryopyrin/Nalp3. *Nature* **440,** 233–236 (2006).
28. Li, P. *et al.* Mice deficient in IL-1 β-converting enzyme are defective in production of mature IL-1β and resistant to endotoxic shock. *Cell* **80,** 401–411 (1995).

Supplementary Information is available in the online version of the paper.

Acknowledgements This work was funded by the Dana Foundation (E.L.), the National Institutes of Health (E.L., D.T.G.) and the Deutsche Forschungsgemeinschaft (E.L., M.T.H.). We thank G. Nuñez and V. M. Dixit for providing anti-caspase-1 Abs. We thank B. De Strooper and L. Serneels for the BACE1 knockout mice and discussion. We also thank H. Jacobsen for the BACE1 transgenic mice.

Author Contributions M.T.H, M.P.K, A.S., A.D., S.S., A.V.-S., A.G., D.A., A.R., T.T. and E.L. performed experiments and analysed data, E.G. provided human samples and analysed data, A.H. was involved in study design and analysed data, E.L., M.T.H., M.K. and D.T.G. designed the study and wrote the paper. All authors discussed results and commented on the manuscript.

Author Information Reprints and permissions information is available at www.nature.com/reprints. The authors declare no competing financial interests. Readers are welcome to comment on the online version of the paper. Correspondence and requests for materials should be addressed to E.L. (eicke.latz@uni-bonn.de), M.T.H. (michael.Heneka@ukb.uni-bonn.de) or D.T.G. (douglas.golenbock@umassmed.edu).

©2013 Macmillan Publishers Limited. All rights reserved

METHODS

Animals and ages. APP/PS1 transgenic animals[5] were obtained from The Jackson Laboratory (number 005864) on the C57BL/6 background. NLRP3-deficient animals[27] (Millennium Pharmaceuticals) were backbred onto C57BL/6 mice genotype to more than 99% C57BL/6, which was confirmed by microsatellite analysis. Caspase-1-deficient mice were generated by BASF[28]; these mice were subsequently obtained by M. Starnbach, who provided the mice for this study after 10 generations of backbreeding onto the C57BL/6 background. All mice were housed under standard conditions at 22 °C and a 12 h light:dark cycle with free access to food and water. Animal care and handling was performed according to the Declaration of Helsinki and approved by the local ethical committees. The following animal groups were analysed: WT, *Nlrp3*$^{-/-}$, APP/PS1, APP/PS1/*Nlrp3*$^{-/-}$, *Casp1*$^{-/-}$, APP/PS1/*Casp1*$^{-/-}$.

Human tissue samples. Post-mortem brain materials from histologically confirmed cases of Alzheimer's disease and age-matched controls who had died from non-neurological disease were from the Neurological Tissue Bank of the Biobank from the Hospital Clinic-Institut d'Investigacions Biomèdiques August Pi i Sunyer. Samples from patients with mild cognitive impairment and early-onset Alzheimer's disease were obtained from the Banner Health collection (http://www.bannerhealth.com). Ages and post-mortem sampling times were similar between controls and cases of mild cognitive impairment, early-onset Alzheimer's disease and Alzheimer's disease. Post-mortem times across all cases varied from 1.5 to 5 h. Patients were 75 ± 10 years old.

Behavioural phenotyping. For the Morris water-maze test, spatial memory testing was conducted in a pool consisting of a circular tank (Ø1 m) filled with opacified water at 24 °C. The water basin was dimly lit (20–30 lx) and surrounded by a white curtain. The maze was virtually divided into four quadrants, with one containing a hidden platform (15 × 15 cm), present 1.5 cm below the water surface. Mice were trained to find the platform, orienting by three extra maze cues placed asymmetrically as spatial references. They were placed into the water in a quasi-random fashion to prevent strategy learning. Mice were allowed to search for the platform for 40 s; if the mice did not reach the platform in the allotted time, they were placed onto it manually. Mice were allowed to stay on the platform for 15 s before the initiation of the next trial. After completion of four trials, mice were dried and placed back into their home cages. Mice trained four trials per day for eight consecutive days. For spatial probe trials, which were conducted 24 h after the last training session (day 9), the platform was removed and mice were allowed to swim for 30 s. The drop position was at the border between the third and fourth quadrant, with the mouse facing the wall at start. Data are given as the percentage of time spent in quadrant Q1, representing the quadrant where the platform had been located, and compared with the averaged time the animals spent in the remaining quadrants. In the afternoon of the same day, a visual cued testing was performed with the platform being flagged and new positions for the start and goal during each trial. All mouse movements were recorded by a computerized tracking system that calculated distances moved and latencies required for reaching the platform (Noldus, Ethovision 3.1). For open field exploration, mice were placed in the centre of the dimly lit (20–30 lx) chamber of the open field arena. Animal movements were tracked by an automatic monitoring system (Noldus Ethovision 3.1) for 5 min. The area was virtually divided into a centre (square with 40 cm edge lengths), a corridor (7.5 cm along the walls) and four corner squares (10 cm edge lengths), which partly overlapped with the corridor area. The time spent in each area, horizontal and vertical activity, frequency of urination and defaecation were monitored. The experiment was repeated on three consecutive days. The novel object recognition test was performed according to a previously established protocol with minor changes[29]. Briefly, the test procedure consisted of three sessions: habituation, training and retention. Each mouse was individually habituated to the open field arena. Habituation was allowed for 10 min. One day later, during the training session, two identical objects (object A) were placed into the two opposing corners of the centre area 30 cm apart from each other, and mice were allowed to explore the area and the objects for 10 min. The total time spent exploring both identical objects was recorded to examine place or object preference. Exactly 60 min or 1 day later, during the retention sessions, mice were placed back into the same arena in which one familiar (object A) and one novel object (object B) replacing the second object A were placed. Mice were then allowed to explore freely for 5 min and the time spent exploring each object was recorded. Exploration of the object was considered when the head of the animal was at least facing the object from a minimum distance of 1–2 cm or closer, but recording was cut as soon as mice turned their heads away from the previously investigated object. Time spent exploring the objects during trials was determined and is shown as discrimination ratio (novel object interaction/total object interaction). The arena and all objects were thoroughly cleaned with 70% ethanol solution after each trial.

Electrophysiology. For slice preparation, acute hippocampal transversal slices were prepared from 7- to 9-month-old WT, *Nlrp3*$^{-/-}$, APP/PS1 or combined APP/PS1/*Nlrp3*$^{-/-}$ and APP/PS1/*Casp1*$^{-/-}$ mice according to standard procedures. In brief, mice were deeply anaesthetized and the brain was quickly transferred into ice-cold carbogenated (95% O_2, 5% CO_2) artificial cerebrospinal fluid which contained 125 mM NaCl, 2 mM KCl, 1.25 mM NaH_2PO_4, 2 mM $MgCl_2$, 26 mM $NaHCO_3$, 2 mM $CaCl_2$ and 25 mM glucose. Hippocampi were dissected and cut into 400 μm transverse slices with a vibratome (Leica, VT1200S). Slices were maintained in carbogenated artificial cerebrospinal fluid at room temperature for at least 1.5 h before recording. Recordings were performed in a submerged recording chamber at 32 °C. For electrophysiology, after placing the slices in the submerged recording chamber, field excitatory postsynaptic potentials were recorded in stratum radiatum of CA1 region with a borosilicate glass micropipette (resistance 3–15 MΩ) filled with 3 M NaCl at a depth of 120–200 μm. Monopolar tungsten electrodes were used for stimulating the Schaffer collaterals at a frequency of 0.1 Hz. Stimulation was set to elicit a field excitatory postsynaptic potential with a slope of approximately 40% of maximum for LTP recordings and approximately 60% for long-term depression recordings. After 20 min baseline stimulation, LTP was induced by applying TBS. One burst consisted of four pulses at 100 Hz, repeated 10 times in a 200 ms interval. Three such bursts were used to induce LTP at 0.1 Hz. Basic synaptic transmission and presynaptic properties were analysed by input–output measurements and paired-pulse facilitation. The input–output measurements were performed by application of a defined value (paired-pulse facilitation) of current (25–250 μA in steps of 25 μA) and by adjusting the stimulus intensity to a certain current eliciting a fibre volley of desired voltage. Paired-pulse facilitation was measured by applying a pair of two stimuli in different inter-stimulus-intervals ranging from 10, 20, 40, 80 to 160 ms. Data were collected, stored and analysed with LABVIEW software (National Instruments). The initial slope of field excitatory postsynaptic potentials elicited by stimulation of the Schaffer collaterals was measured over time, normalized to baseline, which was the mean response of the 20 min before TBS application and plotted as average ± s.e.m. Parameters leading to an exclusion of single experiments were (1) an unstable baseline (variability more than ± 10%) or (2) a large population spike after TBS application producing an artefactually large LTP. Paired-pulse facilitation data were analysed by calculation of the ratio of the slope of the second field excitatory postsynaptic potential divided by the slope of the first one. All data were recorded and analysed in a blind fashion.

Tissue preparation. After completion of the behavioural testing, mice were deeply anaesthetized and transcardially perfused with 15 ml phosphate-buffered saline (PBS). The brains were removed from the skull. One hemisphere was frozen immediately for biochemical analysis and the other was either fixed in 4% paraformaldehyde or frozen over a mixture of dry ice and isopentane.

Brain protein extraction. Snap-frozen brain hemispheres were extracted as previously described[25]. Briefly, hemispheres were homogenized in PBS, 1 mM EDTA, 1 mM EGTA, 3 μl ml^{-1} protease inhibitor mix (Sigma). Homogenates were extracted in RIPA buffer (25 mM Tris-HCl, pH 7.5, 150 mM NaCl, 1% NP40, 0.5% NaDOC, 0.1% SDS), centrifuged at 100,000*g* for 30 min and the pellet containing insoluble amyloid-β was solubilized in 2% SDS, 25 mM Tris-HCl, pH 7.5. In addition, the SDS-insoluble pellet was extracted with 70% formic acid in water. Formic acid was removed using a speed vac (Eppendorf) and the resulting pellet was solubilized in 200 mM Tris-HCl, pH 7.5.

Immunohistochemistry. Free-floating 40 μm serial sections were cut on a vibratome (Leica). Sections were stored in 0.1% NaN3, PBS. For immunohistochemistry, sections were treated with 50% methanol for 15 min. Then, sections were washed three times for 5 min in PBS and blocked in 3% BSA, 0.1% Triton X-100, PBS (blocking buffer) for 30 min followed by overnight incubation with the primary antibody in blocking buffer. Specificity controls were performed by staining with the secondary reagent and omission of the primary antibodies. Sections were washed three times in 0.1% Triton X-100, PBS and incubated with Alexa-488- or Alexa-594-conjugated secondary antibodies (1:500, Invitrogen) for 90 min, washed three times with 0.1% Triton X-100, PBS for 5 min. Sections were mounted using Immomount (Thermo). The following primary antibodies were used with respective concentrations: rabbit polyclonal anti-GFAP (1:800, Dako), rat monoclonal anti-mouse CD11b (MCA711, 1:400, Serotec), rabbit polyclonal anti-Iba1 (1:200, Wako), anti-ASC (1:200; AL177, AdipoGen), anti-NLRP3 (1:200; Cryo-2, AdipoGen) and anti-Fizz-1 (1:400 MAB1523, R&D Systems). Fluorescence microscopy was done on an Olympus BX61 equipped with a spinning disk unit or on an A1-MP laser scanning microscope (Nikon). Images were processed in CellˆP 3.5 (Olympus) or in NIS-elements 4 (Nikon). Alternatively, cryosections (20 μm) were fixed in 4% paraformaldehyde and immunostained using antibody IC16 (ref. 30) against human amyloid-β1-15 (1:400) or a specific antiserum against 3NTyr^{10}-Aβ^{25} following the above-described protocol.

Plaque histology. For thioflavin S staining, vibratome sections were rinsed in water, incubated in 0.01% thioflavin S in 50% ethanol and differentiated in 50% ethanol. Sections were analysed using a BX61 microscope equipped with a spinning-disk unit to achieve confocality (Olympus) or an A1-MP laser scanning microscope (Nikon). Image stacks were deconvoluted using CellˆP (Olympus). Quantitative

©2013 Macmillan Publishers Limited. All rights reserved

assessment of plaque areas was done using the MBF-ImageJ 1.43m software bundle (National Institutes of Health). In brief, total plaque number and amyloid-β area fraction were calculated using the software ImageJ 1.43m with plugins from the WCIF ImageJ collection. In particular, images were normalized and an automatic thresholding on the basis of the entropy of the histogram ('MaxEntropy') was used to identify the plaques. Pictures were converted to a binary and the 'fill holes' and 'watershed' algorithm were applied. Finally, plaque number, plaque area and average amyloid-β plaque size were calculated using the 'analyze particles' plugin of ImageJ. The amyloid-β area fraction was determined by dividing total plaque area by the area of the microscopic field. For staining plaques with methoxy-X04, sections were washed with PBS, incubated with 10 μM methoxy-XO4 in 50% DMSO/50% NaCl (0.9%), pH 12 for 10 min and washed twice with PBS before continuing with immunohistochemistry.

Protein blotting. Samples were separated by 4–12% NuPAGE (Invitrogen) using MES or MOPS buffer and transferred to nitrocellulose membranes. For caspase-1 blots, positive and negative controls were generated by precipitating supernatants from WT immortalized murine macrophages. For the negative control, cells were treated with 200 ng ml^{-1} lipopolysaccharide for 4 h. For the positive control, cells were treated with 200 ng ml^{-1} lipopolysaccharide for 3 h, followed by 10 μM nigericin for 1 h. APP and amyloid-β were detected using antibody 6E10 (Covance) and the C-terminal APP antibody 140 (CT15, gift from J. Walter). IDE was blotted using antibody PC730 (Calbiochem), caspase-1 using antibodies Casp1 clone 4B4.2.1 (gift from Genentech) and a caspase-1 antibody raised in rabbit (gift from G. Nuñez), neprilysin using antibody 56C6 (Santa Cruz), tubulin using antibody E7 (Developmental Studies Hybridoma Bank), BACE1 with antibody 2253 (ProSci), NOS2 using antibody 160862 (Cayman Chemicals), and β-actin using A2228 (Sigma) and 926-42212 (LI-COR Biosciences). Immunoreactivity was detected by enhanced chemiluminescence reaction (Millipore) or near-infrared detection (Odyssey, LI-COR). Chemoluminescence intensities were analysed using Chemidoc XRS documentation system (Biorad).

ELISA quantification of cerebral amyloid-β concentrations. Quantitative determination of amyloid-β was performed using an electrochemoluminescence ELISA for amyloid-β_{1-38}, amyloid-β_{1-40} and amyloid-β_{1-42} (Meso Scale Discovery). Signals were measured on a SECTOR Imager 2400 reader (Meso Scale Discovery). For ELISA determination of 3NTyr^{10}-Aβ, Mesocale L15XA 96-well plates were coated with 2 μg ml^{-1} of the monoclonal 3NTyr10-Aβ antibody 4A5E8 (own production) in PBS overnight at 4 °C. Plates were blocked with 5% blocker A (Meso Scale), 0.1% mouse gamma globulin (Rockland). SDS and formic-acid fractions from mouse brain were diluted in 1% blocker A, 0.1% mouse gamma globulin 1:25 and 1:100, respectively. Thirty-microlitre samples were incubated for 4 h at room temperature, washed with Tris wash buffer (Meso Scale) and incubated with 0.25 μg ml^{-1} MSD-tagged antibody 4G8 (Meso Scale) diluted in 1% blocker A, 0.1% mouse gamma globulin for 1 h at room temperature. Wells were washed with Tris wash buffer, and 150 μl of 2× read buffer (Meso Scale) was added.

ELISA quantification of cerebral IL-1β concentrations. Quantitative determination of IL-1β was performed using the MLB00C ELISA for the determination of murine IL-1β according to the protocol of the supplier (R&D Systems).

Quantitative PCR. RNA was extracted from brain tissues using the RNAeasy Micro Kit (Qiagen). Total RNA was quantified spectrophotometrically and reverse transcribed into complementary DNA using the RevertAid First Strand cDNA Synthesis kit (Fermentas) according to the manufacturer's instructions. Real-time quantitative PCR was performed using the StepOnePlus Real-Time PCR System (Applied Biosystems). The TaqMan gene expression assay and TaqMan universal PCR master mix (Applied Biosystems) was used for PCR amplification and real-time detection of PCR products. PCRs were done in 20 μl with 1 μl of the reverse transcribed product corresponding to 40 ng of total RNA, 1 μl of the gene expression assay mix and 10 μl of the master mix with the following temperature profile: 95 °C for 10 min and 45 cycles of 95 °C for 15 s and 60 °C for 1 min. mRNA expression values were normalized to the level of GAPDH expression. The following probes from LifeTechnologies were used: GAPDH (Mm99999915_g1), FIZZ-1 (Mm00445109_m1), NOS2 (Mm00440485_m1), Arg-1 (Mm00475988_m1), IL-4 (Mm00445259_m1), IDE (Mm00473077_m1); for BACE1 detection the following set of primers was used forward: ACAACCTGAGGGGAAAGTCC, reverse: TAC TACTGCCCGTGTCCACC. Analysis of the expression of the genes was performed using StepOne 2.2 software provided by Applied Biosystems.

Determination of amyloid-β-containing plaque-associated microglia. For the determination of amyloid-β-containing plaque-associated microglia, a double immunofluorescence staining for CD11b and amyloid-β used the antibodies described above. Fields of plaques were randomly selected in the cortex. Images were made in Cell-P with automatic illumination. The area of CD11b overlaying plaques was determined with the co-localization finder plugin in Image J 1.43m and corrected for total plaque area determined with the subroutine particle analysis after background subtraction equal for all images and binarization. Only plaques with a diameter smaller than 30 μm were included in the analysis. Per animal, a coverage of 50–200 plaques by microglia was determined. Animal number per group was five.

Assessment of microglial functions *in vivo*. For the *in vivo* amyloid-β phagocytosis assay, mice were intraperitonealy injected 3 h before being killed with 10 mg kg^{-1} methoxy-XO4 (provided by A. Verbruggen) in 50% DMSO/50% NaCl (0.9%), pH 12. Mice were perfused with ice-cold PBS and the brains were removed, chopped into pieces and incubated in HBSS, 10% FCS containing 0.144 mg ml^{-1} collagenase type IV for 1 h at 37 °C. Homogenization was achieved by pipetting gently up and down using a 19-gauge needle. The homogenate was filtered through a cell strainer (70 μm) and centrifuged at 155*g* and 4 °C for 10 min without a brake. The pellet was re-suspended in 9 ml 70% Percoll in PBS and underlayered with ice-cold 10 ml 37% Percoll in PBS and overlayered with 6 ml ice-cold PBS. The gradient was centrifuged at 800*g* and 4 °C for 25 min without a brake. Microglial cells were recovered from the 37/70% Percoll interphase, diluted with 3 vol. PBS and centrifuged at 880*g* and 4 °C for 25 min (Beckman Allegra) without a brake. The pellet containing the microglial cells was re-suspended in 200 μl PBS. For flow cytometry analysis, 50 μl of cells were diluted with 0.5 ml HBSS and centrifuged at 250*g* for 5 min at 4 °C. Binding of antibodies to Fc-receptors was prevented by adding 1 μg Fc-block and incubating for 10 min on ice. Cells were taken up in 50 μl of primary antibody mix (CD11b-APC (1:100, BioLegend, number 101212), CD45-FITC (1:100, eBioscience, number 11-0451), CD36-PE (1:100, eBioscience, number 12-0361)) and incubated for 30 min on ice. Cells were centrifuged at 250*g* for 5 min at 4 °C and re-suspended in 200 μl HBSS. For control and compensation, corresponding isotype control antibodies were used. Cells were measured on a FACSCanto II (BD Bioscience). For analysis, the CD11b$^+$ CD45$^+$ population was gated. WT mice injected with methoxy-XO4 were used to determine the methoxy-X04 threshold for non-phagocytosing cells, and unstained WT cells were used to determine background fluorescence. For FACS, microglia were stained with CD11b alone and sorted using a FACSDiVa cell sorter (BD Bioscience). To determine total brain methoxy-X04 fluorescence, APP/PS1 and APP/PS1/*Nlrp3*$^{-/-}$ were injected with methoxy-X04 as described above. After 3 h, brains were homogenized in PBS with 1 mM 4-(2-aminoethyl) benzenesulphonyl fluoride hydrochloride and 50 μl of the homogenate was measured at 368 nm excitation and 450 nm emission in a black 96-well plate using an infinite 200-plate reader (Tecan).

Immunocytochemistry of sorted microglia. A subset of microglial cells that were isolated according to the procedure described above were used to verify the uptake of methoxy-04 labelled amyloid-β by immunocytochemistry. Therefore, cells were brought onto glass slides by cytospin and subsequently fixed with 4% paraformaldehyde. Intracellular amyloid-β was visualized by double immunostaining for IC16 (ref. 30) and either CD11b (MCA711; AbSerotec) to detect microglial boundaries or LAMP2 using antibody Abl-93 (Developmental Studies Hybridoma Bank) to determine the intracellular localization of methoxy-X04 and IC16 positive amyloid-β. Inflammasome activation was visualized using the same cells and staining for CD11b and anti-ASC (AL177; AdipoGen).

DiOlistics and morphological analysis. Hippocampal neurons from WT, APP/PS1, APP/PS1/*Nlrp3*$^{-/-}$ and APP/PS1/*Casp1*$^{-/-}$ mice were labelled using DiOlistic on acute slices. Briefly, the mice were anaesthetized and decapitated, and the brain was quickly transferred into ice-cold carbogenated (95% O_2, 5% CO_2) artificial cerebrospinal fluid. Hippocampi were dissected and cut into 400 μm transversal slices with a vibratome (VT 1000S, Leica). Vibratome slices were immediately fixed in 4% PFA overnight at 4 °C. Tungsten particles (50 mg; 1.7 μm in diameter; Bio-Rad) were spread on a glass slide, and 100 μl of dye solution prepared by dissolving 3 mg of lipophilic dye DiI (Invitrogen) in 100 μl of methylenechloride (Sigma-Aldrich). The dried dye-coated particles were removed from the glass slide, re-suspended in 3 ml of distilled water and sonicated. The dye solution was subsequently diluted 1:100. To improve the bead attachment, the tube walls were precoated with a solution of PVP (polyvinyl-pyrrolidone) (stock: 0.05 mg ml^{-1} in ethanol; Bio-Rad), and the bullets were stored at room temperature. Dye-coated particles were delivered to the acute slices using a hand-held gene gun (Bio-Rad, Helios Gene Gun System). A membrane filter (3 μm; Millipore) was inserted between the gene gun and the preparation to prevent clusters of large particles from landing on the tissue. After shooting, slices were kept in PBS for 3 days at room temperature to allow dye diffusion. The slices were postfixed with 4% PFA, washed and mounted using an anti-fading water-based mounting medium (Biomeda). The spine density of pyramidal cells was measured for mid-apical dendrites. The selected dendrite segments were imaged using a LSM510 Meta confocal microscope (Zeiss) using a ×40 water-immersion objective and a zoom 4, and were z-sectioned at 0.5 μm. The number of spines was normalized per micrometre of dendritic length. We analysed statistics using GraphPad Prism 5.03. All data shown are presented as mean and s.e.m. The data obtained were compared between two different experimental conditions using a two-tailed Student's *t*-test. $^*P < 0.05$, $^{**}P < 0.01$, $^{***}P < 0.001$.

©2013 Macmillan Publishers Limited. All rights reserved

29. Bevins, R. A. & Besheer, J. Object recognition in rats and mice: a one-trial non-matching-to-sample learning task to study 'recognition memory'. *Nature Protocols* **1,** 1306–1311 (2006).

30. Jäger, S. *et al.* alpha-secretase mediated conversion of the amyloid precursor protein derived membrane stub C99 to C83 limits Aβ generation. *J. Neurochem.* **111,** 1369–1382 (2009).

©2013 **Macmillan Publishers Limited. All rights reserved**